Aerodynamic Drag Reduction Around Vehicles Using a Curved Deflector

Mohamed Maine[1*], Mohamed El Oumami[2], Otmane Bouksour[2]

[1]Sustainable Innovation and Applied Research Laboratory,
 Universiapolis, Bab Al Madina, Tilila, Agadir, PC: 8143, MOROCCO

[2]Laboratory of Production, Mechanics and Industrial Engineering, Higher School of Technology,
 University Hassan II of Casablanca, km 7, Oasis, Casablanca, PC: 8118, MOROCCO

*Corresponding Author

Abstract: A passive flow control on a generic car model was numerically studied. The Ahmed's model with rear slant angle of 25° was used to study the aerodynamic effects. The concave deflector was tested for the first time in this paper to minimize the drag coefficient. The deflector was fixed between the end of the roof and the top of the rear window. Simulations were firstly performed for different straight deflector's length rates based on the length of the model, for Reynolds number Re=7.89×10⁵ and inlet velocity U_o=40m/s. A significant drag reduction was observed for the high length rate studied. Secondly, the length rate was fixed, and the deflector was investigated for different curvature radius and inclination angles. It was concluded that the Ahmed model with concave deflector gives the best drag reduction, compared to the model with straight deflector and the model without deflector. It was observed that the installation of a concave deflector on the Ahmed model widen the wake zone and remove the vortices from the rear base. For this case, the lift coefficient was reduced, this improves the stability of vehicle on the road at high speed.

Keywords: Aerodynamic drag reduction, Ahmed model, curvature radius, deflector, passive drag reduction, passive flow control, CFD

1. Introduction

The industrial world is today in perpetual evolution and the demand for energy continues to increase. Much of this energy was consumed by means of transportation. Energy needs are increasing in both developed and emerging countries and even in developing countries. Alongside this, there are new requirements and environmental concerns that are needed in terms of pollution reduction and compliance with environmental protection standards. These two aspects directly concern car manufacturers. This is why they are moving towards optimizing current technologies or proposing new technologies to reduce vehicle consumption and/or air pollution. For ground vehicles, the energy consumption depends on the speed of the ride. According to Eulalie, from 65 km/h, the part of the air resistance remains lower than the energy used to move the mass of the car [1]. This aerodynamic resistance increases rapidly to over 90 % at high speeds [2]. The reduction of energy consumption needs the optimization of the car's shape so that it does not oppose the aerodynamic efforts on the road. Several parts of the vehicle contribute to aerodynamic training (mirrors, wheels, rear glasses, rear base). Hucho and Sovran show that the detachment field in the rear end of the car contributes to more than 40 % of aerodynamic training [3].

Research has focused a lot on controlling the flow around moving machines [4]. For motor vehicles, there are two methods of reducing the aerodynamic drag of cars: active and passive methods [5], [6]. The active method consists of

installing devices in specific locations at specific angles, in order to modify the vortices generated in the wake zone: Synthetic jets [7]; Pulsed jets [8], [9], [10], [11]; Steady blowing micro jets at the top edge of slanted surface [12], [13], [14], [15] ; Suction [16], [17], [18] ; Plasma actuators [19] and fluid oscillators [20]. The passive method consists on the use of discrete obstacles, added around or on the roof of the vehicle to change the vortices that are created in the wake zone: Tail plate [21]; Non-smooth surface [22] ; Rear screen and rear fairing [23] ; Underbody device [24] ; Vortex generators on the roof of the model [25], [26], [27]; Streaks [28] ; Jet boat tail [29] ; Rear linking tunnels [30]; Lateral guide vanes [31] ; Underbody diffusers [32], [33], [34] ; Vertical splitter plate [35] and deflector at the edges of the slanted surface and vertical base [36], [37], [38], [39]. Relative to active control, passive control method does not need any sophisticated actuators and electronic control systems, which insures higher reliability. Furthermore, the passive control method has another obvious advantage since it does not need any power input [40]. In this paper, the study will focus on the use of a deflector as a passive method of reducing the aerodynamic drag of cars.

Much work has been carried out on the control of the wake flow using a deflector installed on the rear slant angle at 25° of the Ahmed models as in Table 1. Fourrié et al. analyzed the effect of a deflector fixed between the end of the roof and the top of the rear window on both the separated zone and the longitudinal vortices [36]. Hanfeng et al. investigated the effects of the position, relative height, and width of deflectors on the aerodynamic drag [37]. The works of Raina et al. aimed firstly to numerically evaluate flow over a 3D bluff body using deflector plate at the rear end, and secondly, explored the effect of additional flow velocities on drag coefficient [38],[39].

Different conditions were used in these works. Fourrié et al. and Hanfeng et al. perform an experimental study on the deflector installed at rear slant of Ahmed model for Reynolds numbers between 7.7×10^5 and 8.7×10^5 [36], [37]. Raina et al. did a numerical study using RANS model with two different turbulence equations (SST k-ω and k-ε), for Reynolds numbers between 7.7×10^5 and 9.4×10^5 [38], [39]. Fourrié et al. and Raina et al. used a scale model of 1:1 while Hanfeng et al. used a scale model of 1:2. The deflector's angle varied from 0° to 5°. The aerodynamic drag reduction is between 6.6 and 11.8 %. The values of drag coefficient obtained from the two turbulence models are vastly different. Maybe this variation is due to the lack of prediction of the sublayer. It was observed that the drag is influenced by the inclination angle of the deflector and the Reynolds number.

In previous studies, authors were using plate deflector. Their decision variables are focused on the angle of inclination and the flow velocity. They suggest that flow control on such geometries should take into account any flow structures that contribute to the model wake flow. The study of the variation of deflector's length and curvature depending to inclination angle is treated, to our knowledge, for the first time, in this article in order to determine the best concave deflector that minimizes the aerodynamic drag.

This paper is divided in this introductory section and other five sections. Section 2 defines the model of simulation. Section 3 gives the mathematical background of our numerical study which is detailed in section 4. Data for simulation using the ANSYS software is presented in this last section. Results and discussion were reported in section 5 aiming an optimization of geometric parameters of a curved deflector by studying the minimization of drag coefficient of Ahmed body model. A conclusion and some perspectives for future development works were drawn in Section 6.

Table 1 - Research work on the Ahmed model with deflector

Author, year	A-Fourrié et al. 2011 [36]	B-Hanfeng et al. 2016 [37]	C-Raina et al. 2017 [38]	D-Raina et al. 2018 [39]
Model	Ahmed model with rear slant angle of 25°			
Deflector's angle	5°	0°	5°	5°
deflector's dimensions	389×20×1.2	194.5×10×1.2	389×20×1.2	389×20×1.2
Study	Experimental	Experimental	Numerical	Numerical
Turbulence equations	--	--	SST k-ω	k-ε
Reynolds number R_e	7.7×10^5	8.7×10^5	7.7×10^5	9.4×10^5
Inlet velocity U_o (m/s)	40	25	40	50
Drag coefficient C_d	0.259	0.381	0.318	0.271
Reference*	0.285	0.432	0.340	0.290
% reduction	9 %	11.8 %	7 %	6.6 %

* C_d for Ahmed model with rear slant angle of 25° without deflector

2. Model of Simulation

2.1 Ahmed Model

The complexity of the study of flows around cars requires a simple and standard model to compare the results of different numerical and experimental studies. Ahmed et al. proposed a simplified land vehicle model for a better analysis and understanding three-dimensional air flows around the vehicle [40]. Several authors have used Ahmed's model as a reference for studying the aerodynamics of ground vehicles [6]. It is a generic car geometry comprising a front plate with rounded parts and a clean sloping rear upper surface. The angle of inclination is adjustable and is the main variable parameter of the model in the experimental research of Ahmed [6]. Most of the body drag is due to the pressure drag that is triggered from the back. The wake structure is very complex with a separation zone and counter-rotating vortices generated on the intersection between the rear slant angle and lateral edges. The dimensions of Ahmed model are 1044×389×288 mm. The lower surface of Ahmed's model is 50 mm above the ground, and four legs are used to support the model. The origin of the coordinates is fixed on the ground at the medium point of the rear surface and the directions of the coordinates are as in **Fig. 1**. In this way, the rear base is inclined at 25°.
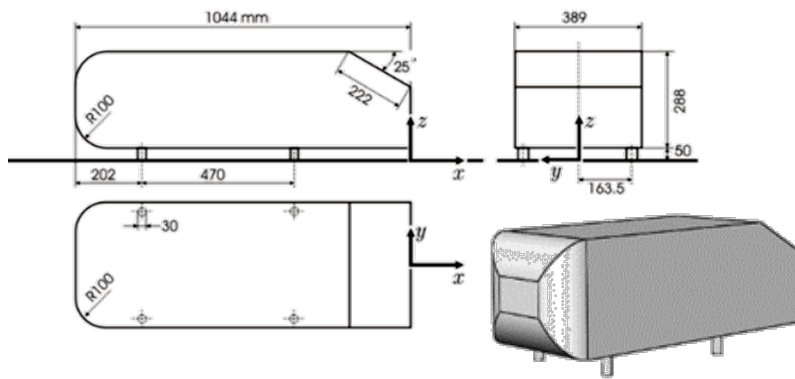

Fig. 1 - Ahmed model (left) dimensions, (right) 3D Geometry [40]

2.2 Deflector

The deflector is a device installed on the rear base of the Ahmed model. The deflector is 0.389 m width. The length varies between 0 mm (without deflector) and 195 mm. The thickness is 1.2 mm and the deflector corners are cut at 45° as in Fig. 2. The deflector has a recessed connection with the Ahmed model.
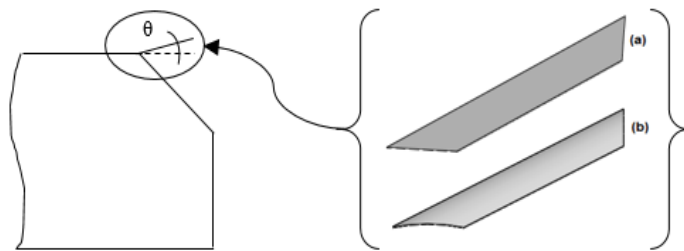

Fig. 2 - Deflector installed on the rear slant of Ahmed model (a) straight deflector; (b) concave deflector

3. Mathematical Model

3.1 Navier-Stokes Equations

Since the flow was considered incompressible (the energy balance does not intervene), the flow is governed by the mass balance equation:

$$\frac{\partial \rho}{\partial t} + \frac{\partial}{\partial x_i}(\rho u_i) = 0 \tag{1}$$

In addition, by the momentum balance equation:

$$\frac{\partial u_i}{\partial t} + u_j \frac{\partial u_i}{\partial x_j} = -\frac{1}{\rho}\frac{\partial P}{\partial x_i} + v\frac{\partial^2 u_i}{\partial x_i \partial x_j} \qquad (2)$$

Where u is the freestream velocity, ρ the specific density, P the average value of the pressure and v the kinematic viscosity of the fluid.

3.2 RANS Turbulence Models

3.2.1 Reynolds Average

This average describes the velocity fields statistically. The turbulent flow is divided into two terms:

$$u_i = U_i + u_i' \qquad (3)$$

Where U_i is the average value of the freestream velocity and u_i' is its fluctuation compared to the average value U_i (with $U_i = \overline{u_i}$ and $\overline{u_i'} = 0$). The average of this decomposition therefore makes it possible to remove the fluctuating variables. The average was applied to the two previous Navier-Stokes equations "Eq. (1) and (2)" by decomposing the variables u and P. These equations become:

$$\frac{\partial U_i}{\partial x_i} = 0 \qquad (4)$$

$$\frac{\partial U_i}{\partial t} + U_j \frac{\partial U_i}{\partial x_j} = -\frac{1}{\rho}\frac{\partial P}{\partial x_i} + v\frac{\partial^2 U_i}{\partial x_i \partial x_i} - \frac{\partial \overline{u_i' u_j'}}{\partial x_j} \qquad (5)$$

An additional term appeared, namely $-\frac{\partial \overline{u_i' u_j'}}{\partial x_j}$. One approach for closing these equations is to use the Boussinesq approximation defined as:

$$-\rho\overline{u_i' u_j'} = \mu_t \left(\frac{\partial u_i}{\partial x_j} + \frac{\partial u_j}{\partial x_i}\right) - \frac{2}{3}\left(\rho k + \mu_t \frac{\partial u_k}{\partial x_k}\right)\delta_{ij} \qquad (6)$$

Where: μ_t is the turbulent viscosity, k is the turbulent kinetic energy and δ_{ij} is the Kronecker symbol. The turbulent viscosity μ_t can be obtained by solving additional transport equations. The number of these equations depends on the chosen turbulence model. In this work, the emphasis will be on the k-ω (SST) model [41].

3.2.2 Turbulence Model K-Ω (SST)

The k-ω SST (Shear Stress Transport) model developed by Menter combines the precision of the k-ω model in the near wall and the k-ε model in the far field region. Such an approach was made by transforming the model k-ε into a formulation k-ω with the addition of a blending function between the two regions [42]. The k-ω (SST) model is capable of modeling a wide range of flow profiles with increased precision. The transport equations for the k-ω (SST) model are given as follows:

$$\frac{\partial}{\partial t}(\rho k) + \frac{\partial}{\partial x_i}(\rho k u_i) = \frac{\partial}{\partial x_j}\left[\Gamma_k \frac{\partial k}{\partial x_j}\right] + \tilde{G}_k - Y_k \qquad (7)$$

$$\frac{\partial}{\partial t}(\rho \omega) + \frac{\partial}{\partial x_i}(\rho \omega u_i) = \frac{\partial}{\partial x_j}\left[\Gamma_\omega \frac{\partial \omega}{\partial x_j}\right] + G_\omega - Y_\omega + D_\omega \qquad (8)$$

$\tilde{G}_k$ and G_ω represent the production conditions of k and ω. Y_k and Y_ω represent the terms of dissipation of k and ω. Γ_k and Γ_ω represent the effective diffusivity of k and ω. Finally, D_ω represents the term of cross diffusion. The turbulent kinetic energy (k) and specific dissipation rate (ω) are determined as follows:

$$k = \frac{3}{2}(U_0 I)^2 \tag{9}$$

$$\omega = \rho \frac{k}{\mu} \left(\frac{\mu_t}{\mu}\right)^{-1} \tag{10}$$

Where U_0 is the inlet velocity and I the turbulence intensity. A blending function F_1, between the near wall region and the far field was integrated in the terms of the production derivation, dissipation, diffusivity, and cross diffusion as follows:

$$\emptyset = F_1 \emptyset_1 + (1 - F_1)\emptyset_2 \tag{11}$$

Where $\emptyset_1$ groups all the constants of the original k-ω model and $\emptyset_2$ groups all the constants of the transformed k-ε model. $\emptyset$ is the resulting constant of the model and F_1 is the blending function, which is equal to 1 in the near wall and 0 far from the surface [42].

3.3 Aerodynamics Coefficients

The determination of the air constraints on the car consists of measuring the components of the aerodynamic torsor which are [1]:

3.3.1 Drag Coefficient

It is the ratio of the aerodynamic torsor, to the dynamic pressure relative to the reference speed, on the projected surface in the main flow direction. It is defined as:

$$C_D = \frac{F_x}{\frac{1}{2}\rho U_0^2 S_x} \tag{12}$$

With F_x is the drag force, ρ is the fluid density of the flow, U_0 is the inlet velocity, and S_x is the projected area in the vehicle flow direction.

3.3.2 Lift Coefficient

The lift coefficient describes the vehicle's support linked to aerodynamics. It is an important safety parameter concerning handling on fast roads. Similarly, for the force F_z, the lift coefficient is defined as:

$$C_L = \frac{F_z}{\frac{1}{2}\rho U_0^2 S_x} \tag{13}$$

4. Numerical Study

4.1 Geometry and Mesh of The 3D Model

A 3D model was created and simulated on the ANSYS software. For stationary flow, to minimize the processing time, the domain is cuted in half from the plane of symmetry XOZ. The dimensions of the simulation domain are 11044×1194.5×1839 mm. The inlet velocity was 3.26 L upstream and 6.32 L downstream. The upper far-field boundary is 1.5 L and the domain width is 1 L (were L is the model's length). These dimensions are recommended by the ERCOFTAC workshop on Refined Turbulence Modelling [43]. These dimensions of the computational domain implies a blocking factor equal to 5.23 %. To capture flow on boundary layer, a coefficient of $y^+ = 1$ was chosen. The first layer thickness was 0.0083 mm. The grid expansion ratio from the boundary layer of the model is $\frac{\Delta x_i}{\Delta x_{i+1}} = 1.2$. The elements are hexahedral type near the contours of the model and the road, and tetrahedral type in the far field region as in Fig. 3. The boundary conditions are presented in Table 2.
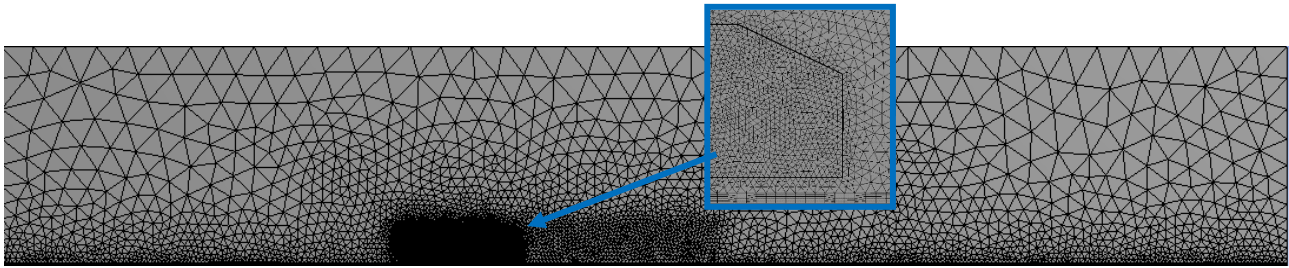
Fig. 3 - Air domain of Ahmed model

Table 2 - Boundary conditions

Zone	Boundary conditions	Inputs parameters
Upstream	Velocity-Inlet	$u_x = U_0 \ ; u_y = 0 \ ; u_z = 0$
Downstream	Pressure-Outlet	free
Road	Wall	$u_x; u_y; u_z = 0$
Top	Wall	$u_x; u_y; u_z = 0$
Symmetry	Symmetry	$u_x = U_0 \ ; u_y = 0$
Side	Wall	$u_x; u_y; u_z = 0$
Ahmed model	Wall	$u_x; u_y; u_z = 0$

4.2 Mesh Sensitivity and Numerical Study

To ensure a grid independent solution for all simulations, a mesh sensitivity study was done on the Ahmed model without deflector, at a Reynolds number of 7.89×10^5. Three meshes M1, M2 and M3 were used: coarse, medium and fine, respectively. The percentages of difference for two successive meshes of the drag coefficient (C_D) and the lift coefficient (C_L) were less than 3 % as in Table 3. For M2 (664 818 elements), increasing the number of elements by 53.1 % to obtain M3 (1 417 521 elements), gives 2.88 % variation of (C_D) and 2.22 % variation of (C_L). The "Fig. 4 (a)" shows that all the meshes respect the condition of $y^+ < 1$. The numerical results of velocity profile at X= -163 mm "Fig. 4 (b)" are compared to experimental data of Lienhart [44]. The obtained results show a good convergence with the mesh refinement and also a good agreement with experiments. It can be seen that a mesh independence solution was obtained for M2. Hence, this mesh will be used for all other simulations. Numerical calculations were performed on a CPU of 3 processors and 8 GB of RAM. The residuals of the continuity, velocity and k-ω equations are limited to 10^{-6}.

Table 3 - Results of the mesh sensitivity study

Mesh	No. elements	Drag coefficient (C_D)	Difference	Lift coefficient (C_L)	Difference
M1	287 819	0.3001	6.07 %	0.2651	19.94 %
M2	664 818	0.2819	2.88 %	0.3180	2.22 %
M3	1 417 521	0.2738	--	0.3251	--

5. Results and Discussion

After analyzing the flow around Ahmed model without deflector in the first phase for three meshes (M1, M2 and M3) and Reynolds number $Re = 7.89 \times 10^5$ corresponding to inlet velocity $U_0 = 40 \ m.s^{-1}$, the values of medium mesh (M2) are compared with literature data as in Table 4. The difference of drag coefficient obtained compared to Thomas and Agarwal k-ω SST [45] and Guilimineau EARSM [46] are respectively 2.46 % and 0.53 %. These low differences are due to the grid and number of elements used. For experimental data, a difference of 1.09 % was observed compared to Ahmed et al. [40] and 5.92 % compared to Meile et al. [47]. For the lift coefficient, excluding Guilimineau's result, which is aberrant compared to others, the minimal difference observed with our result is 1.55 %, compared to Thomas et Agarwal k-ω SST numerical study [45], and 7.83 % compared to Meile experimental study [47]. The second phase of this study focuses on the Ahmed model with a deflector. The length was varied from 20 to 195 mm, for Reynolds number $Re = 7.89 \times 10^5$ corresponding to inlet velocity $U_0 = 40 \ m.s^{-1}$. The

length was represented by the rate l_D/L [%], where l_D is the deflector's length and L the Ahmed model length. The simulation results show that the deflector's length influences the aerodynamic coefficients as in Table 5.

Table 4 - Results comparison of drag and lift coefficients

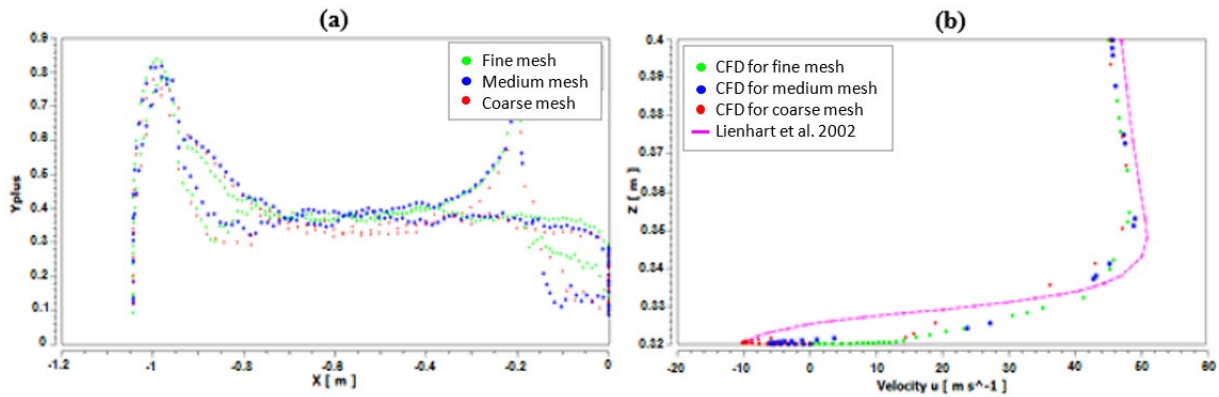|	Drag coefficient (C_D)	Lift coefficient (C_L)
Present work	0.2819	0.3180
Thomas and Agarwal, k-ω SST [45]	0.2890	0.3230
Guilmineau et al., EARSM [46]	0.2804	0.0083
Ahmed et al., Experiments [40]	0.2850	--
Meile et al., Experiments [47]	0.2990	0.3450

Fig. 4 - Mesh sensitive study (a) y+ around the Ahmed model for different meshes; (b) velocity profile at X= -163 mm

Table 5 - Drag and lift coefficients of the Ahmed model for different rates of deflector length

l_D/L [%]	Deflector's length [m]	Drag coefficient (C_D)	Lift coefficient (C_L)
1.92	0.02	0.2919	0.0871
3.83	0.04	0.2828	0.0288
5.75	0.06	0.2752	-0.0152
7.66	0.08	0.2745	-0.0226
9.58	0.10	0.2737	-0.0353
11.50	0.12	0.2710	-0.0538
13.40	0.14	0.2701	-0.0557
15.33	0.16	0.2667	-0.0875
17.24	0.18	0.2670	-0.0650
18.67	0.195	0.2636	-0.0610

The variation of aerodynamic coefficients was shown in Fig. 5. For the drag coefficient, a deflector's length rate of 1.92 % was compared to literature. The differences observed were: 8.21 % with k-ω numerical study of Raina [38], 7.71 % with k-ε numerical simulation of Raina [39] and 12.7 % with experimental study of Fourrié [36]. The difference with the average value of the three authors mentioned above was only 3.25 %. For other deflector's length rates, the drag coefficient decreases with the increase of deflector's length rate. The best drag reduction of 6.94 % was observed for the maximum rate 18.67 %. Moreover, the lift coefficient decreases with the increase of deflector's length rate. It has been observed that the deflector has the advantage of decreasing the lift coefficient, which can be used to stabilize the vehicle on the road at high speed. The turbulent kinetic energy (TKE) in the symmetry plane for the Ahmed model with a deflector of different lengths is shown in Fig. 6. The maximum TKE is located around the lowest separation in the wake's model. For the model without deflector, the TKE production is located behind the body on the floor. The region with a high TKE value was at about X = 0.15 m. The use of a deflector reduces the TKE and moves its location away. For deflector's length rate less than 10 %, the region of TKE began from the rear slant angle of the model to wake zone. The high TKE values are more intense and located between X=0.1 m and X=0.3 m. For deflector's length rate greater than 10 %, a maximum TKE production is located at the position between X=0.2 m and X=0.3 m; its value is lower than that for deflector's length rate less than 10 %.
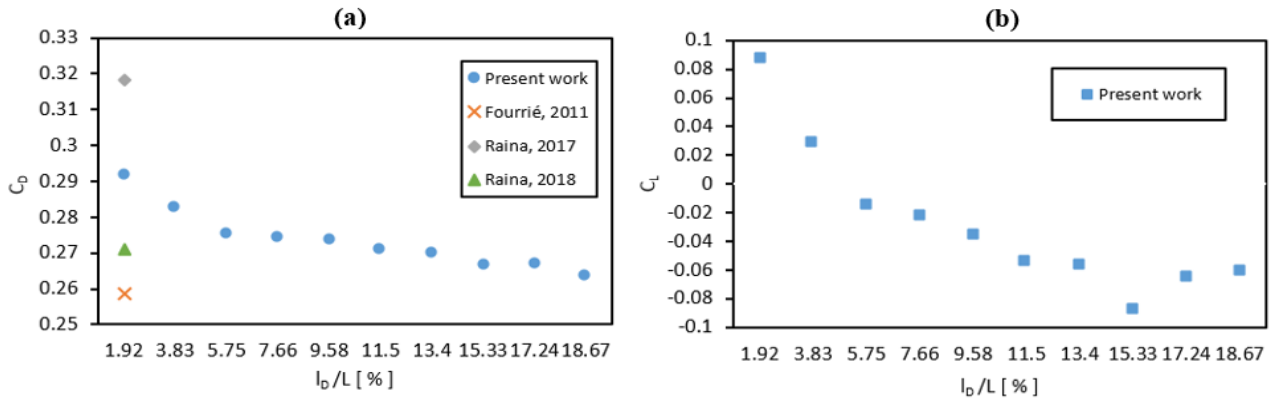
Fig. 5 - Aerodynamics coefficients of Ahmed model with a deflector with different lengths (a) drag coefficient; (b) lift coefficient

Table 6 - Variation of deflector's dimensions for length rate of 5.76 %

ID	R [m]	α [m]	θ [°]	C_D	C_L
1			0	0.2711	0.0187
2			1	0.2746	0.0312
3	0.4505	0.001	2	0.2718	0.0239
4			3	0.2772	0.0143
5			4	0.2725	0.0047
6			5	0.2709	-0.0111
7			0	0.2727	0.0283
8			1	0.2695	0.0378
9	0.226	0.002	2	0.2725	0.0529
10			3	0.2687	0.0355
11			4	0.2683	-0.0023
12			5	0.2690	-0.0160
13			0	0.2696	0.0678
14			1	0.2774	0.0508
15	0.1515	0.003	2	0.2690	0.0404
16			3	0.2728	0.0240
17			4	0.2734	0.0097
18			5	0.2714	-0.0043
19			0	0.2711	0.0848
20			1	0.2715	0.0797
21	0.1145	0.004	2	0.2699	0.0410
22			3	0.2698	0.0263
23			4	0.2688	0.0102
24			5	0.2687	0.0032
25			0	0.2730	0.0358
26			1	0.2737	0.0512
27	0.0925	0.005	2	0.2705	0.0473
28			3	0.2698	0.0384
29			4	0.2774	0.0308
30			5	0.2748	0.0081
31			0	0.2760	0.0720
32			1	0.2750	0.0763
33	0.078	0.006	2	0.2751	0.0665
34			3	0.2772	0.0656
35			4	0.2753	0.0430
36			5	0.2774	0.0360

For real ground vehicles, the deflector's length is limited by the design of the vehicle. A deflector's length rate less than 6 % can be considered reasonable. To find the best shape for the deflector, an analysis will be made of the effect of a deflector bend on aerodynamic drag. An arc shape has been studied in Fig. 7. The deflector's length rate of 5.75 % was chosen and the curvature radius was calculated by the equation (14).

$$R = \frac{\alpha^2 + \beta^2}{2\alpha}$$

(14)

Where R is the radius of curvature, β is the half of deflector's length $\left(\beta = \frac{l_D}{2}\right)$ and α is the curvature's arrow. The concave curvature was chosen for values of α between 0.001 m and 0.006 m. The curvature radius for different values of α are between 0.4505 m and 0.078 m. The angle of inclination θ of the deflector varied between 0° and 5° as in Table 6.
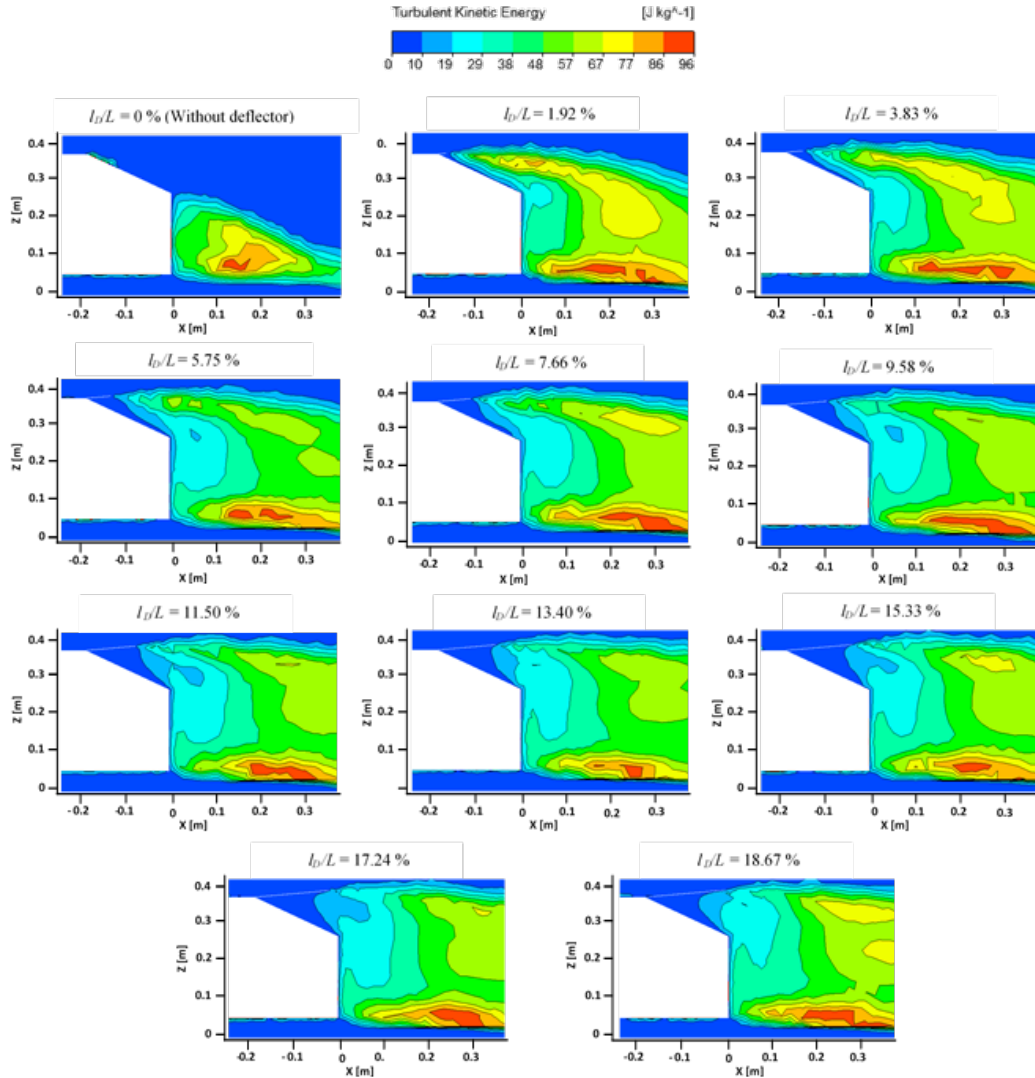

Fig. 6 - Turbulent kinetic energy in the symmetry plane Y = 0 for different deflector's length rates
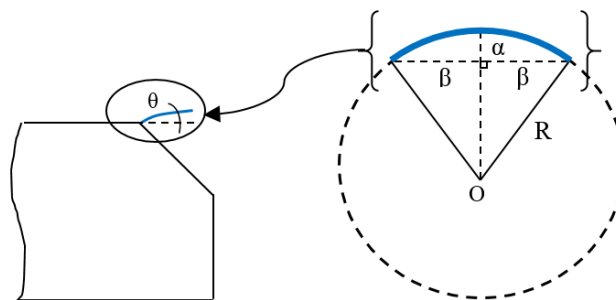
Fig. 7 - Deflector with curvature installed at the slant angle of Ahmed model

The aerodynamics coefficients were presented in the Fig. 8. It was observed that the drag coefficient was influenced by the curvature of the deflector. The minimum drag observed is for the curvature radius of 0.226 m and inclination angle θ of 4°. The drag reduction observed for this type of deflector, compared to Ahmed model without deflector, was 4.82 % (the reduction was 2.51 % compared for the straight deflector). This is due to the further increase in the size of the central wake at the rear end of the body. Regarding the lift coefficient, the values decrease with the increase of the inclination angle and becomes negative for θ = 5° (stabilizing effect for the vehicle). To improve the study, the inclination angle was refined around the optimal radius of curvature. θ was varied from 3° to 5° with a step of 0.5°. The results of simulation are presented in Table 7. For the drag coefficient, the values decrease at θ = 3.5° then increase; the optimal value observed was 0.2673. It can be assumed that there must be a strong modification in the flow behavior at this deflector angle. The drag reduction observed for this configuration of the curved deflector compared to the straight one was 2.87 % (5.18 %, compared to the Ahmed model without deflector). The lift coefficient decreases to a negative value with the increase of inclination angle. The minimum coefficient observed was -0.0247 for θ = 4.5° as in Fig. 9.
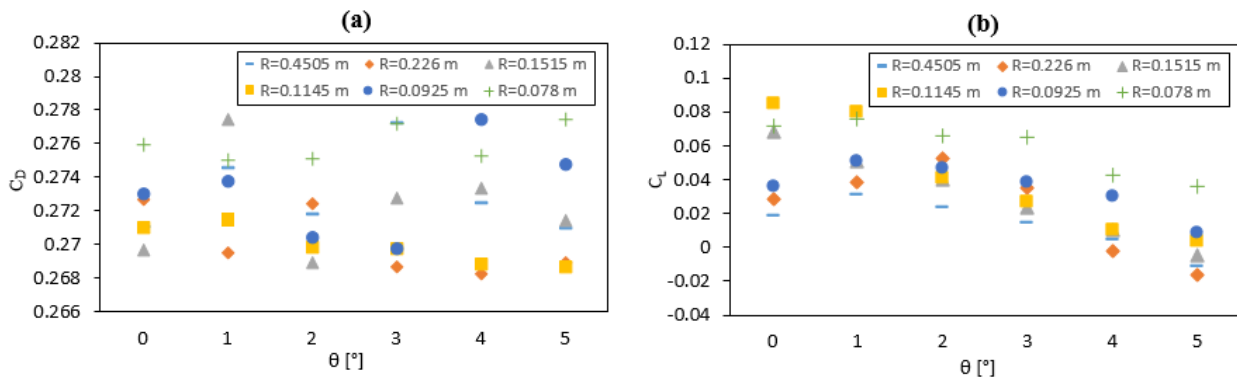
Fig. 8 - Aerodynamic coefficients of the Ahmed model with a deflector with different radius of curvature and angles of inclination for a length ratio of 5.76 % (a) drag coefficient; (b) lift coefficient

Table 7 - Aerodynamics coefficients of deflector around the optimum radius of curvature

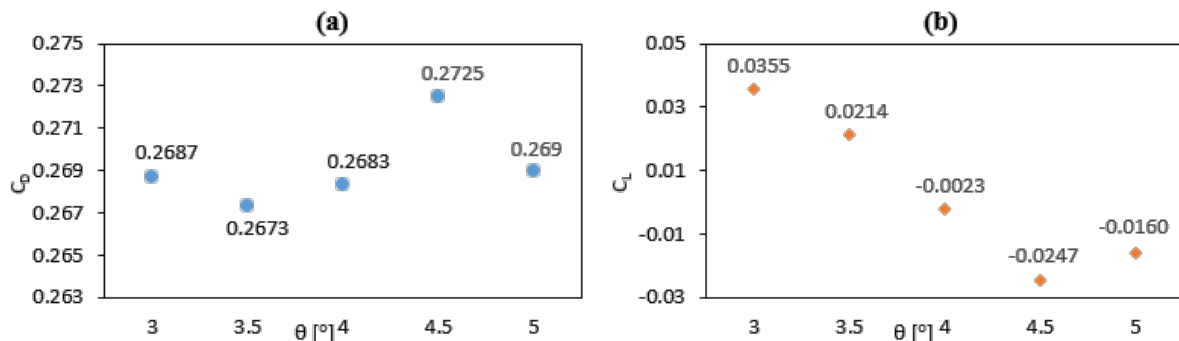| ID	R [m]	α [m]	θ [°]	C_D	C_L
1			3	0.2687	0.0355
2			3.5	0.2673	0.0214
3	0.226	0.002	4	0.2683	-0.0023
4			4.5	0.2725	-0.0247
5			5	0.2690	-0.0160

Fig. 9 - Aerodynamics coefficients of deflector around the optimum radius of curvature R = 0.226 m (a) drag coefficient; (b) lift coefficient

Fig. 10 presents a comparison of turbulent kinetic energy in the symmetry plane of the Ahmed model for three cases (without deflector, with deflector's rate of 5.75 % in straight case and with optimal curvature's deflector). It was observed that the maximum TKE was located closer to the base of the model. For the first case (body without deflector), the TKE is high in the bottom of the model near the ground in the wake body between X = 0.1 m and X = 0.2 m. In this case, the size of main vortices was increased. In the second case (body with straight deflector's rate of 5.75 %), the wake zone has been lengthened and the vortices were dissipated. For the last case (body with deflector's

rate of 5.75 % and radius curvature of 0.226 m), a maximum TKE was moved away from the model and located in the position X = 0.3 m. It can see that the use of the deflector delays separation and disturbs the vortices, which minimizes the depression created in the wake zone behind the vehicle, then reduces its aerodynamic drag. The installation of a concave deflector on the Ahmed model increases the separated region over the model rear window, widen the wake zone and remove the vortices from the rear base. This reduces the turbulent speed as well as the pressure created by the flow of the boundary layer; and so minimize aerodynamic drag. These results complement those found by Fourrié [36], Hanfeng [37] and Raina [38], [39] to approve the capability of deflector concave to reduce aerodynamics drag and its capacity to improve the vehicle stability on the road at high speed.
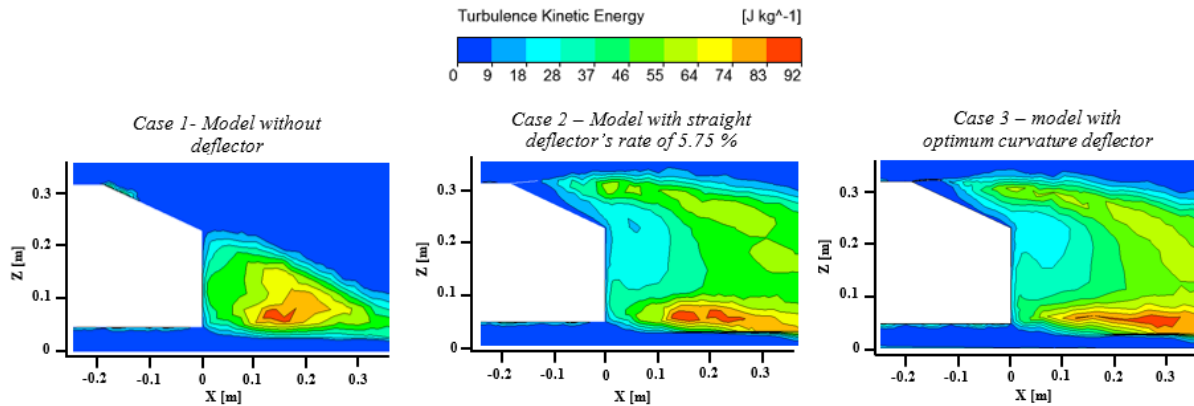
Fig. 10 - Turbulent kinetic energy in the symmetry plane Y = 0 of the Ahmed models with deflector in different cases

6. Conclusion

The minimization of drag coefficient of the Ahmed model using concave deflector was studied for the first time in this paper. The Ahmed model with rear slant angle of 25° was investigated numerically, for Reynolds number Re=7.89×10^5 and inlet velocity U$_o$=40m/s. A deflector with length rate (deflector's length / car's length) between 1.92 % and 18.67 % was tested. The RANS turbulence model with the two equations SST k-ω was used in this study. The results show that increasing the length of the deflector reduces aerodynamic drag. The maximum length ratio studied (18.67 %) gives the best configuration and minimizes aerodynamic drag up to 6.90 %, compared to Ahmed model without deflector. The widening of the rear flow region disrupts the development of longitudinal vortices rotating in opposite directions on the side edges of the rear window.

The installation of the deflector on passenger cars is however limited by design constraints (aesthetics of the vehicle). The rate of length of the deflector of 5.75 %, compared to the vehicle length, was chosen to study the effects of the curvature radius and the inclination angle on the reduction of aerodynamic drag. The concave deflector with inclination angle of 3.5° and curvature radius of 0.226 m was the best configuration. The drag reduction observed was about 2.87 % compared to Ahmed model with straight deflector, while the global reduction was 5.18 % compared to the body without deflector. In addition, the lift coefficient was reduced, that improved the stability of vehicles on the road at high speed. This study suggests that efficient flow control strategies around such geometry should take into account all the vortex structures interacting in the wake flow.

This study will be developed using the design of experiments to study the deflector factors that most influence the aerodynamic drag of Ahmed's body in order to find the best combination of curvature, input speed and deflector length. In perspective, we can also consider a deflector that adapts to the speed of the vehicle.

Acknowledgement

References

[1]   Eulalie, Y. (2014). Étude aérodynamique et contrôle de la traînée sur un corps de Ahmed culot droit (Doctoral dissertation, Bordeaux).

[2]   Blocken, B., & Toparlar, Y. (2015). A following car influences cyclist drag: CFD simulations and wind tunnel measurements. Journal of Wind Engineering and Industrial Aerodynamics, 145, 178-186. doi: 10.1016/j.jweia.2015.06.015.

[3]   Hucho, W., & Sovran, G. (1993). Aerodynamics of road vehicles. Annual review of fluid mechanics, 25(1), 485-537.

[4]   Noor A. Ahmed. (2018). From the Dawn of Aerodynamic Science to Modern Flow Control: a Brief Review. International Review of Aerospace Engineering (IREASE), 11, 112-119, doi: 10.15866/irease. v11i3. 13847.

[5]   Sudin, M. N., Abdullah, M. A., Ramli, F. R., Musthafah M. T., & Shamsudin, S. A., (2014). Review of research on vehicles aerodynamic drag reduction methods. Int. J. Mech. Mechatron. Eng., 14, 35-47.

[6]   Maine, M., El Oumami, M., Bouksour, O., & Tizliouine, A. (2019). Review of research on cars wake flow control methods to reduce aerodynamic drag. International journal of innovation and applied studies, 25(3), 1069-1089.

[7]   Kourta, A., & Leclerc, C. (2013). Characterization of synthetic jet actuation with application to Ahmed body wake. Sens. Actuators Phys., 192, 13-26, doi: 10.1016/j.sna.2012.12.008.

[8]   Bideaux, E., Bobillier, P., Fournier, E., Gilliéron, P., El Hajem, M., Champagne, J. Y., Gilotte, P., & Kourta, A. (2011). Drag reduction by pulsed jets on strongly unstructured wake: towards the square back control. Int. J. Aerodyn., 1, 282-298.

[9]   Joseph, P., Amandolese, X., Edouard C., & Aider, J.-L. (2013). Flow control using MEMS pulsed micro-jets on the Ahmed body. Exp. Fluids, 54, 1-12, doi: 10.1007/s00348-012-1442-x.

[10]   Barros, D., Ruiz, T., Borée J., & Noack, B., (2014). Control of a three-dimensional blunt body wake using low and high frequency pulsed jets. Int. J. Flow Control, 6, 61-74, doi: 10.1260/1756-8250.6.1.61.

[11]   Barros, D., Borée, J., Noack, B. Spohn. R. A., & Ruiz, T. (2016). Bluff body drag manipulation using pulsed jets and Coanda effect. J. Fluid Mech., 805, 422-459, doi: 10.1017/jfm.2016.508.

[12]   Wassen, E., Eichinger, S., & Thiele, F. (2010). Simulation of active drag reduction for a square-back vehicle. In Active Flow Control II (pp. 241-255). Springer, Berlin, Heidelberg.

[13]   Aubrun, S., McNally, J., Alvi, F., & Kourta, A. (2011). Separation flow control on a generic ground vehicle using steady microjet arrays. Experiments in fluids, 51(5), 1177-1187.

[14]   Heinemann, T., Springer, M., Lienhart, H., Kniesburges, S., Othmer, C., & Becker, S. (2014). Active flow control on a 1: 4 car model. Experiments in fluids, 55(5), 1-11., doi: 10.1007/s00348-014-1738-0.

[15]   Tebbiche, H., & Boutoudj, M. S. (2021). Active flow control by micro-blowing and effects on aerodynamic performances. Ahmed body and NACA 0015 airfoil. International Journal of Fluid Mechanics Research, 48(2). doi: 10.1615/InterJFluidMechRes.2021036842.

[16]   Moussa, A. A., Yadav, R., & Fischer, J. (2014). Aerodynamic drag reduction for a generic sport utility vehicle using rear suction. Journal of Engineering Research and Applications, 4(8), 101-107.

[17]   Harinaldi, H., Budiarso, B., Warjito, W., Kosasih, E., Tarakka, R., Simanungkalit, S., & Teryanto, I. G. M. (2012). Modification of flow structure over a van model by suction flow control to reduce aerodynamics drag. Makara Journal of Technology, 16(1), 15-21.

[18]   Tarakka, R., Salam, N., Jalaluddin, J., & Ihsan, M. (2018). Active Flow Control by Suction on Vehicle Models with Variations on Front Geometry. International Review of Mechanical Engineering, 12(2), 128-134.

[19]   Shadmani, S., Nainiyan, S. M., Ghasemiasl, R., Mirzaei, M., & Pouryoussefi, S. G. (2018). Experimental study of flow control over an Ahmed body using plasma actuator. Mechanics and Mechanical Engineering, 22(1), 239-252.

[20]   Metka, M., & Gregory, J. W. (2015). Drag reduction on the 25-deg ahmed model using fluidic oscillators. Journal of Fluids Engineering, 137(5).

[21]   Sharma, R. B., & Bansal, R. (2013). CFD simulation for flow over passenger car using tail plates for aerodynamic drag reduction. IOSR Journal of Mechanical and Civil Engineering (IOSR-JMCE), 7(5), 28-35.

[22]   Wang, Y., Wu, C., Tan, G., & Deng, Y. (2017). Reduction in the aerodynamic drag around a generic vehicle by using a non-smooth surface. Proceedings of the Institution of Mechanical Engineers, Part D: Journal of Automobile Engineering, 231(1), 130-144. doi: 10.1177/0954407016636970.

[23]   Sirenko, V., Pavlovs' ky, R., & Rohatgi, U. S. (2012, July). Methods of reducing vehicle aerodynamic drag. In Fluids Engineering Division Summer Meeting (Vol. 44755, pp. 97-102). American Society of Mechanical Engineers.

[24]   Cho, J., Kim, T. K., Kim, K. H., & Yee, K. (2017). Comparative investigation on the aerodynamic effects of combined use of underbody drag reduction devices applied to real sedan. International Journal of Automotive Technology, 18(6), 959-971. doi: 10.1007/s12239-017-0094-5.

[25]   Aider, J. L., Beaudoin, J. F., & Wesfreid, J. E. (2010). Drag and lift reduction of a 3D bluff-body using active vortex generators. Experiments in fluids, 48(5), 771-789. doi: 10.1007/s00348-009-0770-y.

[26]   Yang, X., Hu, Y., Gong, Z., Jian, J., & Liu, Z. (2022). Numerical Study of Combined Drag Reduction Bases on Vortex Generators and Riblets for the Ahmed Body using IDDES Methodology. Journal of Applied Fluid Mechanics, 15(1), 193-207. doi: 10.47176/JAFM. 15.01. 32832.

[27]   Arya, S., Goud, P., Sharma, V., & Mathur, S. (2017). Simulation of passenger car by attaching add-on device to reduce drag force by CFD approach. International Research Journal of Engineering and Technology.

[28]   Pujals, G., Depardon, S., & Cossu, C. (2010). Drag reduction of a 3D bluff body using coherent streamwise streaks. Experiments in fluids, 49(5), 1085-1094.

35

[29]   Hirst, T., Li, C., Yang, Y., Brands, E., & Zha, G. (2015). Bluff body drag reduction using passive flow control of jet boat tail. SAE International Journal of Commercial Vehicles, 8(2015-01-2891), 713-721. doi: 10.4271/2015-01-2891.

[30]   Mohammadikalakoo, B., Schito, P., & Mani, M. (2020). Passive flow control on Ahmed body by rear linking tunnels. Journal of Wind Engineering and Industrial Aerodynamics, 205, 104330.

[31]   Wahba, E. M., Al-Marzooqi, H., Shaath, M., Shahin, M., & El-Dhmashawy, T. (2012). Aerodynamic drag reduction for ground vehicles using lateral guide vanes. CFD letters, 4(2), 68-79.

[32]   Kang, S. O., Jun, S. O., Park, H. I., Song, K. S., Kee, J. D., Kim, K. H., & Lee, D. H. (2012). Actively translating a rear diffuser device for the aerodynamic drag reduction of a passenger car. International Journal of Automotive Technology, 13(4), 583-592. doi: 10.1007/s12239-012-0056-x.

[33]   Marklund, J., Lofdahl, L., Danielsson, H., & Olsson, G. (2013). Performance of an automotive under-body diffuser applied to a sedan and a wagon vehicle. SAE International Journal of Passenger Cars-Mechanical Systems, 6(2013-01-0952). doi: 10.4271/2013-01-0952.

[34]   Huminic, A., & Huminic, G. (2017). Aerodynamic study of a generic car model with wheels and underbody diffuser. International Journal of Automotive Technology, 18(3), 397-404. doi: 10.1007/s12239-017-0040-6.

[35]   Gilliéron, P., & Kourta, A. (2010). Aerodynamic drag reduction by vertical splitter plates. Experiments in fluids, 48(1), 1-16. doi: 10.1007/s00348-009-0705-7.

[36]   Fourrié, G., Keirsbulck, L., Labraga, L., & Gilliéron, P. (2011). Bluff-body drag reduction using a deflector. Experiments in Fluids, 50(2), 385-395. doi: 10.1007/s00348-010-0937-6.

[37]   Hanfeng, W., Yu, Z., Chao, Z., & Xuhui, H. (2016). Aerodynamic drag reduction of an Ahmed body based on deflectors. Journal of Wind Engineering and Industrial Aerodynamics, 148, 34-44. doi: 10.1016/j.jweia.2015.11.004.

[38]   Raina, A., Harmain, G. A., & Haq, M. I. U. (2017). Numerical investigation of flow around a 3D bluff body using deflector plate. International Journal of Mechanical Sciences, 131, 701-711. doi: 10.1016/j.ijmecsci.2017.08.018.

[39]   Raina, A., & Khajuria, A. (2018). Flow control around a 3d-bluff body using passive device. International Journal of Science and Engineering, 4(1), 8-13.

[40]   Ahmed, S. R., Ramm, G., & Faltin, G. (1984). Some salient features of the time-averaged ground vehicle wake. SAE Transactions, 473-503. doi: 10.4271/840300.

[41]   Pang, A. L. J., Skote, M., & Lim, S. Y. (2016). Modelling high Re flow around a 2D cylindrical bluff body using the k-ω (SST) turbulence model. Progress in Computational Fluid Dynamics, an International Journal, 16(1), 48-57.

[42]   Menter, F. R. (1994). Two-equation eddy-viscosity turbulence models for engineering applications. AIAA journal, 32(8), 1598-1605. doi: 10.2514/3.12149.

[43]   Manceau, R., Bonnet, J. P., Leschziner, M., & Menter, F. (2002). Proc. 10th ERCOFTAC (SIG-15)/IAHR/QNET-CFD Workshop on Refined Turbulence Modelling" add at the end "Laboratoire d'études aérodynamiques, UMR CNRS 6609, Université de Poitiers, France, October 10–11, 2002.

[44]   Lienhart, H., Stoots, C., & Becker, S. (2002). Flow and turbulence structures in the wake of a simplified car model (ahmed modell). In New results in numerical and experimental fluid mechanics III (pp. 323-330). Springer, Berlin, Heidelberg. To be replaced by : Lienhart, H., Stoots, C., & Becker, S. (2002). Flow and turbulence structures in the wake of a simplified car model (ahmed modell). In : Wagner, S., Rist, U., Heinemann, HJ., Hibig, R. (eds) New results in numerical and experimental fluid mechanics III (pp. 323-330). Notes on Numerical Fluid Mechanics (NNFM), Vol 77. Springer, Berlin, Heidelberg. https://doi.org/10.1007/978-3-540-45466-3_39.

[45]   Thomas, B., & Agarwal, R. K. (2019). Evaluation of various RANS turbulence models for predicting the drag on an Ahmed body. In AIAA Aviation 2019 forum (p. 2919).

[46]   Guilmineau, E., Deng, G. B., Leroyer, A., Queutey, P., Visonneau, M., & Wackers, J. (2018). Assessment of hybrid RANS-LES formulations for flow simulation around the Ahmed body. Computers & Fluids, 176, 302-319. doi: 10.1016/j.compfluid.2017.01.005.

[47]   Meile, W., Brenn, G., Reppenhagen, A., Lechner, B., & Fuchs, A. (2011). Experiments and numerical simulations on the aerodynamics of the Ahmed body. CFD letters, 3(1), 32-39.